

Preparation of sodalite at room temperature with varying hydrogel Al₂O₃/SiO₂ molar ratio for enhanced Cd²⁺ adsorption

X. Zhang*, Y. H. Sun, Y. Huang, J. L. Li, Y. Chen

Key Laboratory of Micro-Nano Materials for Energy Storage and Conversion of Henan Province, Institute of Surface Micro and Nano Materials, College of Chemical and Materials Engineering, Xuchang University, Henan 461000, China

Sodalite crystals were prepared with varying hydrogel Al₂O₃/SiO₂ molar ratio at room temperature via hydrothermal method. The particulate properties of products prepared under room temperature and elevated temperature condition were compared. The results displayed that spherical particles built of small crystallites were obtained after 10 h of room-temperature hydrothermal treatment; while with the same gel composition, the sodalite obtained for 10 h at 90 °C was large lepispherical particles. Moreover, the samples prepared at room temperature exhibited much higher Cd²⁺ sorption capacities, and the maximum adsorption capacities of Cd²⁺ were tested to be 84.2, 88.6, 92.9, and 98.2 mg/g for the sodalite synthesized with hydrogel Al₂O₃/SiO₂ molar ratios of 0.43, 0.55, 0.68 and 0.84, respectively. The reasons can be due to its specific porous structure, large surface area, and more adsorption active sites. Additionally, the kinetics and isotherm analysis revealed that pseudo-second order model and Langmuir model agreed well with the adsorption processes. This work offered an economic synthesis method of sodalite to achieve efficient Cd²⁺ removal from aqueous solution.

(Received December 10, 2023; Accepted April 3, 2024)

Keywords: Sodalite, Nanocrystalline, Cd²⁺ adsorption, Kinetic model, Isotherm

1. Introduction

Given the population health and social sustainable development, people have been actually increasingly aware of environmental problems. Cd²⁺ is one of the most hazardous metal pollutants. Even though very small amounts of Cd²⁺ are ingested, it can easily result in renal dysfunction, hepatic injury, lung damage and hypertension [1,2]. Recently, more attentions are focused on the Cd²⁺ removal from aqueous solutions, some techniques have been employed [3-6]. Among these methods, adsorption is a common method for removing Cd²⁺ with the advantages of simple operation and high removal efficiency. Zeolites provide adsorbents that are environmentally friendly, renewable, and cost-effective [7,8].

Zeolites are porous aluminosilicates consist of tetrahedral SiO₄⁴⁻ and AlO₄⁵⁻. Out of the various zeolites, sodalite possesses a cubic *Im3m* crystal symmetry consisting of a six-membered ring with a pore size of 2.8 Å [9]. Due to its unique structure, sodalite has attracted considerable attentions for the potential applications in optical materials, hydrogen storage, catalyst supports, and waste management [10-13]. According to the reported documents, sodalite may be prepared from various precursor materials and methods [14,15]. In general, these syntheses are carried out at temperatures range 90-150 °C for some time.

Most applications of zeolite crystals are strongly dependent on the frameworks. However, size and shape of samples also play major roles in the efficiency and mode of their applications [16]. Nowadays, many efforts have been aimed at the exploration of various factors which control the particle properties of zeolite products. These results display that the gel chemical composition is a key factor in controlling sample properties [17,18]. Here, we synthesized sodalite with varying hydrogel Al₂O₃/SiO₂ molar ratio at room temperature. The particulate properties (crystal size,

* Corresponding author: zxx5973428@163.com
<https://doi.org/10.15251/DJNB.2024.192.503>

crystal shape) of zeolite products prepared under room temperature and high temperature condition (90 °C, 10 h) were compared. Moreover, the adsorption properties of as-synthesized samples were evaluated by removing Cd²⁺ ions, kinetic model and adsorption isotherm were used for exploring the adsorption processes.

2. Experiments

2.1. Preparation of sodalite

Sodalite crystal was prepared via a hydrothermal synthesis method at room temperature. Sodium aluminate (anhydrous, Merck) and sodium hydroxide (99%, Merck) were dissolved in deionized water. Then colloidal silica (ZS-30, 30 wt%SiO₂) was slowly added to the above solution with vigorous agitation, the resultant hydrogels of molar composition 5.5 Na₂O: x Al₂O₃: 1.0 SiO₂: 80 H₂O (x=0.15, 0.43, 0.55, 0.68, 0.84 and 1.15). The mixture was agitated for 40 min, then placed into autoclaves and hydrothermally crystallized for 10 h at 25 °C. The synthesized samples were marked as SOD-0.15, SOD-0.43, SOD-0.55, SOD-0.68, SOD-0.84 and SOD-1.15, respectively. As a comparison, an experiment was also performed for 10 h at 90 °C with the gel composition x=0.55, the product obtained was denoted SOD-0.55-90 °C. Finally, the powders were recovered, washed with deionized water, followed by drying for 12 h at 95 °C.

2.2. Characterization and analyses

X-ray diffraction (XRD) analysis was conducted by a Philips PW 1830 diffractometer using Cu-K α radiation in 5-45° (2 θ). Scanning electron microscopy (SEM) was taken on a LEO 1530 TFE microscope. Fourier transform infrared (FTIR) transmittance spectra were collected on a Bruker IFS 66 v/s FTIR spectrometer by KBr wafer technique. N₂ adsorption-desorption experiments were carried out at 77K using a Quantachrome Nova 2000e analyzer.

2.3. Cd²⁺ adsorption on zeolite samples

The kinetic adsorption experiments were carried out by a thermostatic oscillator. More specifically, zeolite particles (0.1 g) and 100 mL cadmium nitrate solution (Cd²⁺ concentration 250 mg/L, pH=5.5) were poured into a 150 mL conical flask, shaken at 250 rpm at 25 °C. The Cd²⁺ concentrations in solutions were tested using an atomic adsorption spectrophotometer (PerkinElmer, 900F, USA) with various contact times. The amount of adsorbed Cd²⁺ (q_t, mg/g) was expressed by Eq. (1).

$$q_t = \frac{(C_0 - C_t)V}{M} \quad (1)$$

where C_t and C₀ are the time-dependent and initial Cd²⁺ ions concentrations (mg/L), M is the amount of sodalite adsorbent (g), while V is the solution volume (L).

The adsorption equilibrium experiments were conducted as follows: 0.1 g of each zeolite and 100 mL cadmium nitrate solutions with various Cd²⁺ concentrations (pH=5.5) were poured into a 150 mL conical flask, shaken at 250 rpm at 25 °C. The Cd²⁺ concentration in each solution was tested after 5 h.

3. Results and discussion

3.1. Characterization

3.1.1. XRD analysis

Fig. 1 displays the XRD patterns of products prepared in different Al₂O₃ from 5.5 Na₂O: x Al₂O₃: 1.0 SiO₂: 80 H₂O after 10 h crystallization. From Fig. 1, the product obtained at Al₂O₃/SiO₂=0.15 is poorly crystallized sodalite. With the hydrogel Al₂O₃/SiO₂ ratios increase from 0.43 to 0.84, well-crystallized sodalite products are observed. Obviously, the structure

rearrangement happens and leads to the formation of zeolite nuclei, appropriate Al/Si atomic ratios favor a well-tuned precursor generation. Also, with increasing sodium aluminate in gel mixture, the corresponding high concentration of Al^{3+} benefits small silicate species such as 6-membered rings formation. However, as $\text{Al}_2\text{O}_3/\text{SiO}_2=1.15$, a low diffraction peak intensity of sodalite phase is observed. Compared with sodalite sample obtained for 10 h crystallization at 90 °C with gel composition $\text{Al}_2\text{O}_3/\text{SiO}_2=0.55$, significant broadening and low XRD peak intensities are observed in products prepared at room temperature, indicating that small zeolite crystals are generated.

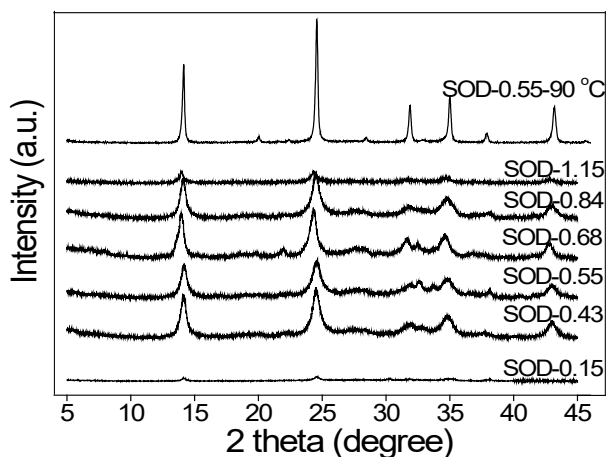


Fig. 1. XRD patterns of samples prepared from the gel mixture with various $\text{Al}_2\text{O}_3/\text{SiO}_2$ molar ratios.

3.1.2. FTIR analysis

The FT-IR spectra of products synthesized from $\text{Al}_2\text{O}_3/\text{SiO}_2$ molar ratios of 0.43, 0.55, 0.68 and 0.84 are displayed in Fig. 2. All the products clearly exhibit sodalite characteristic bands, which are asymmetric stretch of T-O-T (T=Si, Al) at 993 cm^{-1} , symmetric stretch of T-O-T at 737, 710, and 662 cm^{-1} , characteristics of bending vibration of O-T-O at 461 cm^{-1} and 426 cm^{-1} [12,19]. The band corresponds to OH appears at 1658 cm^{-1} . However, compared with the sample obtained under elevated temperature condition, all the framework vibrations of sodalities prepared at room temperature seem to be much broader and less intense, caused by a lower degree of perfection of the nanocrystalline samples [20].

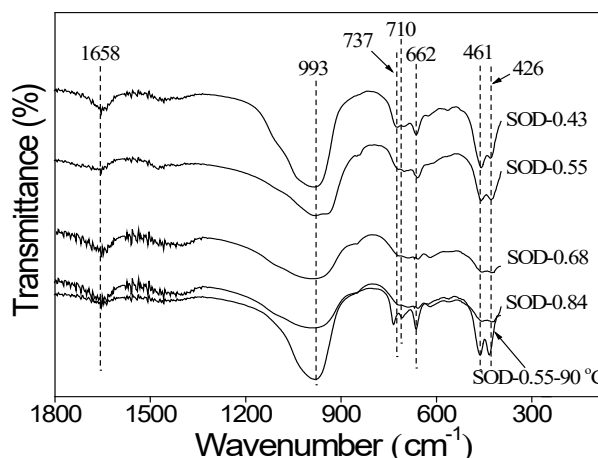


Fig. 2. IR spectra of samples prepared from the gel mixture with various $\text{Al}_2\text{O}_3/\text{SiO}_2$ molar ratios.

3.1.3. SEM analysis

The corresponding SEM images are displayed in Fig. 3. From Fig. 3, the $\text{Al}_2\text{O}_3/\text{SiO}_2$ ratio has an important impact on particle size and morphology of final product. It is clearly seen that the products synthesized at $\text{Al}_2\text{O}_3/\text{SiO}_2=0.43$ and 0.55 are composed of aggregated particles (Fig 3a-b); spherical particles consist of many closely packed nanocrystals with a size of 50-80 nm are observed at $\text{Al}_2\text{O}_3/\text{SiO}_2$ ratio of 0.68 (Fig 3c-d); while as $\text{Al}_2\text{O}_3/\text{SiO}_2=0.84$, wool ball-like crystals built of many nanorods with diameter of 10 nm, length of 100 nm are obtained (Fig 3e). These results are in good agreement with relatively broadening X-ray diffraction peaks, implying that samples consisting of very small crystallites, as expected. It is also observed that the sample obtained for 10 h at 90°C is big lepispherical particles (Fig. 3f). As a result, the crystal growth processes under room-temperature condition can differ from the synthesis at elevated temperature. The reasons can be due to very slow Ostwald ripening and more abundant nucleation at low temperature, thus relatively small crystallites are formed [21].

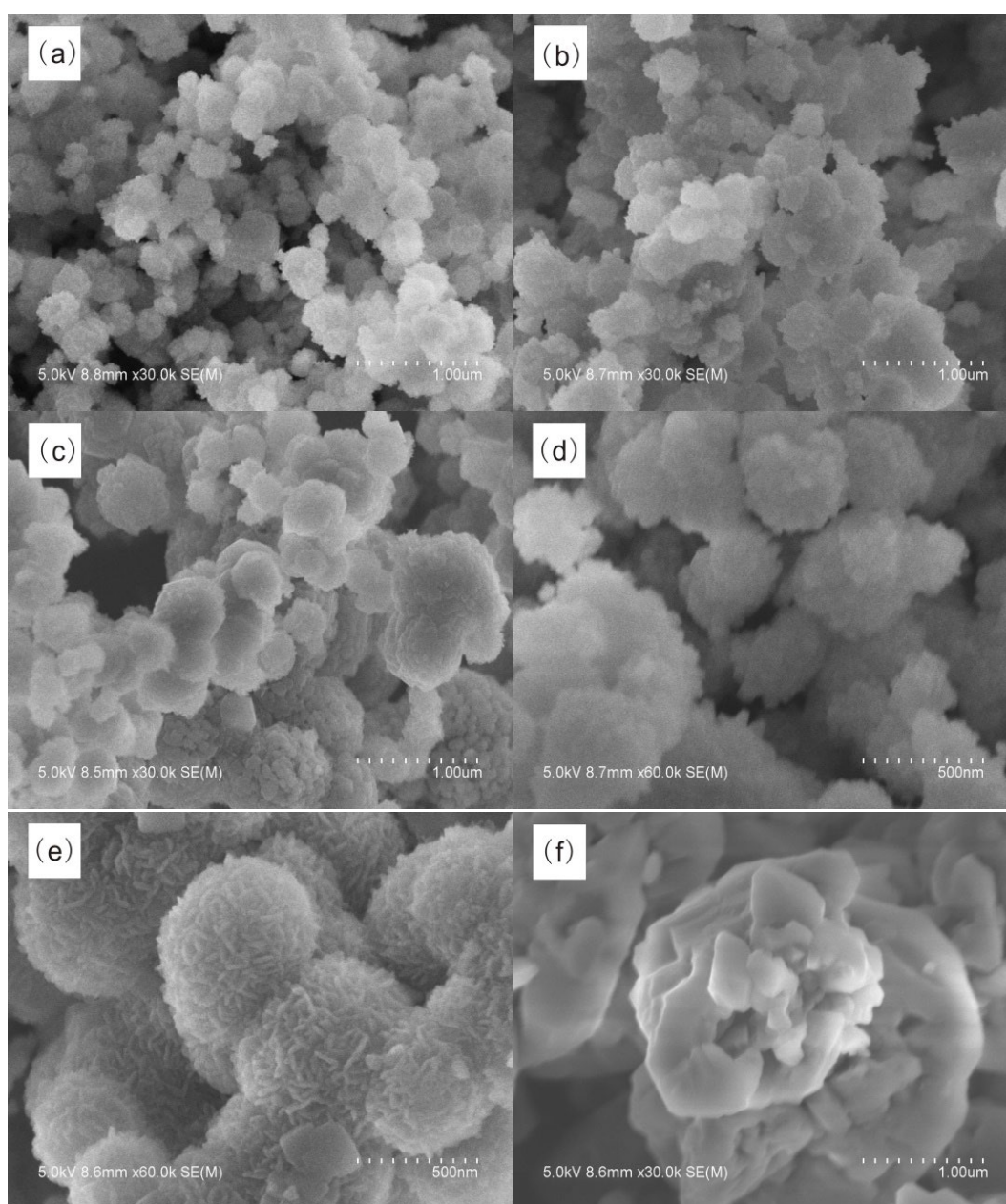


Fig. 3. SEM images of samples prepared from the gel mixture with various $\text{Al}_2\text{O}_3/\text{SiO}_2$ molar ratios. (a) SOD-0.43, (b) SOD-0.55, (c and d) SOD-0.68, (e) SOD-0.84, and (f) SOD-0.55-90 °C.

Additionally, high $\text{Al}_2\text{O}_3/\text{SiO}_2$ ratio favors the formation of individual smaller zeolite nanocrystals, which may further result in larger congregated agglomerates generation. The differences in shape and size are attributed to different levels of Al affect polymerization supersaturation degree, state and distribution of aluminium species in hydrogel, which lead to different number and distribution of pre-nuclei in the reactants [22]. The aggregation growth seems in favour of zeolitic stabilization.

3.1.4. N_2 adsorption-desorption isotherms

Fig. 4 displays the N_2 adsorption-desorption isotherms of as-synthesized samples. It shows a type I hysteresis loop for the elevated temperature crystallization product; while the samples synthesized at room temperature exhibit a type IV with hysteresis loop values 0.5-0.9 (p/p_0), which is characteristic of mesoporous material [23,24]. The mesopores are determined by the aggregation of nanoparticles in the products. Moreover, the products prepared at room temperature have much higher adsorption capacity, and this arises from much smaller primary particles and lower packing densities. These results are agreement with the SEM determinations.

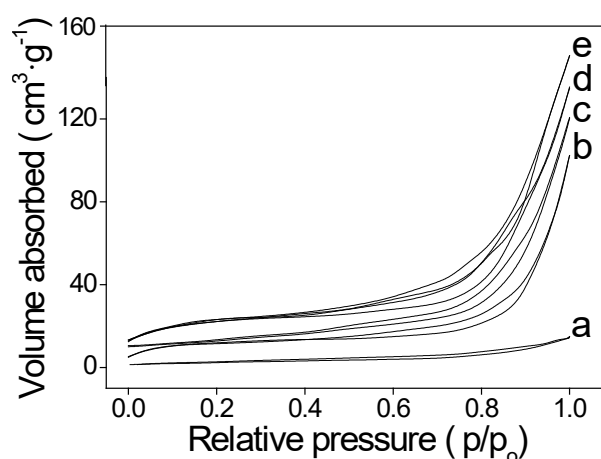


Fig. 4. N_2 adsorption-desorption isotherms of as-synthesized samples. (a) SOD-0.55-90 °C, (b) SOD-0.43, (c) SOD-0.55, (d) SOD-0.68, and (e) SOD-0.84.

3.2. Cd^{2+} adsorption on sodalite products

3.2.1. Adsorption kinetics

The sodalite products of SOD-0.43, SOD-0.55, SOD-0.68, SOD-0.84, and SOD-0.55-90 °C are used as adsorbents to remove Cd^{2+} from aqueous solutions. The influences of contact time on Cd^{2+} adsorption by the five zeolite samples is displayed in Fig. 5. From Fig. 5, the amounts of adsorbed Cd^{2+} increase rapidly within contact time from 0 to 4 h, then increase gradually until equilibrium is attained after 5 h. It is seen that the samples obtained with high $\text{Al}_2\text{O}_3/\text{SiO}_2$ ratios in gel mixture show better adsorption capacity for Cd^{2+} . At this time, the equilibrium adsorption capacities of SOD-0.43, SOD-0.55, SOD-0.68 and SOD-0.84 toward Cd^{2+} are 71.1, 76.3, 80.9 and 85.7 $\text{mg}\cdot\text{g}^{-1}$, respectively. Meanwhile, an adsorption amount of 64.6 $\text{mg}\cdot\text{g}^{-1}$ is obtained on SOD-0.55-90 °C.

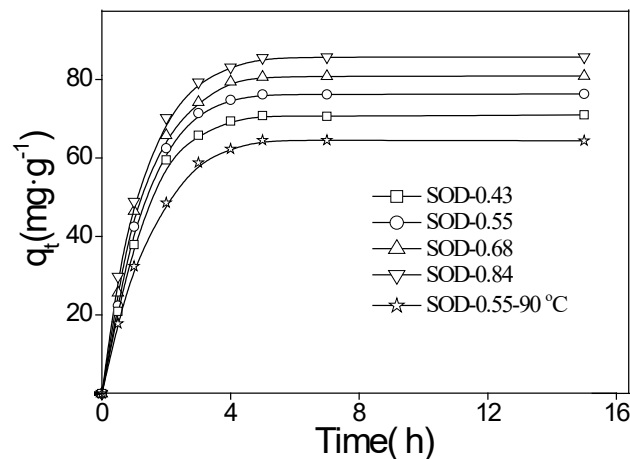


Fig. 5. Influences of contact time on Cd^{2+} adsorption.

Additionally, the pseudo-first order and pseudo-second order kinetic equations are exhibited by Eq. (2) and Eq. (3).

$$\ln(q - q_t) = \ln q - K_1 t \quad (2)$$

$$t/q_t = 1/(K_2 q_e^2) + t/q_e \quad (3)$$

where q_e and q_t are the adsorption capacities at equilibrium and at time t , respectively (mg/g); k_1 ($1/\text{h}$) and k_2 [$\text{g}/(\text{mg}\cdot\text{h})$] are the adsorption rate constants.

The two kinetic models are tested by adopting linearized method, the kinetic parameters and fitted results are exhibited in Table 1 and Fig. 6. Obviously, the R_2^2 correlation coefficients (>0.99) are higher than R_1^2 for every sodalite samples, and the q_e values obtained by the pseudo-second order model are closer to the experimental values. Consequently, it is deduced that adsorption kinetics of zeolite samples for Cd^{2+} follow pseudo-second order model, and the adsorption process of Cd^{2+} on sodalite samples is chemical adsorption [25]. The high adsorption performance of adsorbent can be due to its specific porous structure, large surface area, and more adsorption active sites [26]. Moreover, quick diffusion of target in the adsorbent material is also essential to increase the economics and efficacy of waste water treatment.

Table 1. Kinetic parameters for Cd^{2+} adsorption on the five adsorbents.

adsorbents	Pseudo-first order			Pseudo-second order		
	$q_e/$ ($\text{mg}\cdot\text{g}^{-1}$)	$k_1/$ h^{-1}	R_1^2	$q_e/$ ($\text{mg}\cdot\text{g}^{-1}$)	$k_2/$ ($\text{g}\cdot\text{mg}^{-1}\cdot\text{h}^{-1}$)	R_2^2
SOD-0.43	66.4	0.0811	0.905	58.5	0.0369	0.997
SOD-0.55	72.9	0.0778	0.944	62.7	0.0512	0.996
SOD-0.68	78.2	0.0772	0.932	68.5	0.0526	0.994
SOD-0.84	84.3	0.0755	0.926	76.9	0.0563	0.997
SOD-0.55-90 °C	59.6	0.0758	0.924	52.1	0.0342	0.995

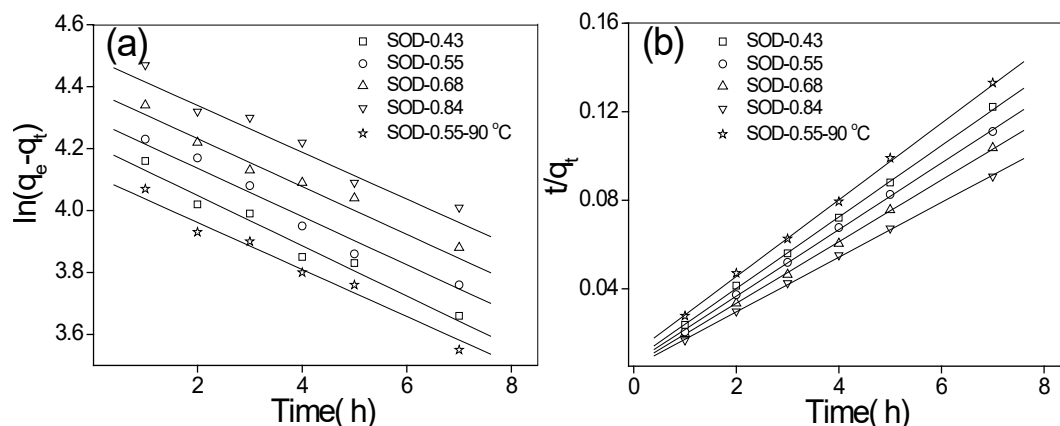


Fig. 6. Pseudo-first order (a) and pseudo-second order (b) kinetics for Cd^{2+} adsorption on zeolite samples.

3.2.2. Adsorption isotherms

The interactions of Cd^{2+} solutions with zeolite adsorbents are explored, corresponding adsorption data are analyzed by Freundlich and Langmuir isotherms following Eq. (4) and Eq. (5).

$$\ln q = 1/n \cdot \ln C_e + \ln K_F \quad (4)$$

$$C_e/q_e = 1/(q_0 K_L) + C_e/q_0 \quad (5)$$

where C_e is the equilibrium of Cd^{2+} concentration (mg/L); q_0 is the maximum Cd^{2+} adsorbed (mg/g); q_e is the amount of Cd^{2+} adsorbed on zeolite adsorbent (mg/g); K_F and $1/n$ are Freundlich isotherm constants referring to the adsorption capacity and adsorption intensity; K_L is the Langmuir constant.

The adsorption parameters were listed in Table 2, and corresponding adsorption isotherms are displayed in Fig. 7. The adsorption isotherms of all the zeolite samples are well explained by Langmuir model with higher R^2 than Freundlich model, implying that Cd^{2+} adsorption happens via monolayer adsorption [27]. Additionally, the maximum Cd^{2+} adsorption capacities (q_0) of SOD-0.43, SOD-0.55, SOD-0.68, SOD-0.84 and SOD-0.55-90 °C are 84.2, 88.6, 92.9, 98.2 and 76.3 mg/g, respectively, demonstrating that sodalite samples synthesized at room temperature are competitive with that obtained at elevated temperature condition.

Table 2. Langmuir and Freundlich isotherm parameters.

adsorbents	Langmuir model			Freundlich model		
	$q_0/$ ($\text{mg} \cdot \text{g}^{-1}$)	$k_L/$ ($\text{L} \cdot \text{mg}^{-1}$)	R_L^2	$1/n$	k_F	R_F^2
SOD-0.43	84.2	0.048	0.995	0.0311	77.84	0.958
SOD-0.55	88.6	0.062	0.994	0.0214	82.63	0.960
SOD-0.68	92.9	0.071	0.996	0.0197	88.12	0.954
SOD-0.84	98.2	0.084	0.995	0.0133	95.58	0.928
SOD-0.55-90 °C	76.3	0.035	0.992	0.0402	72.69	0.922

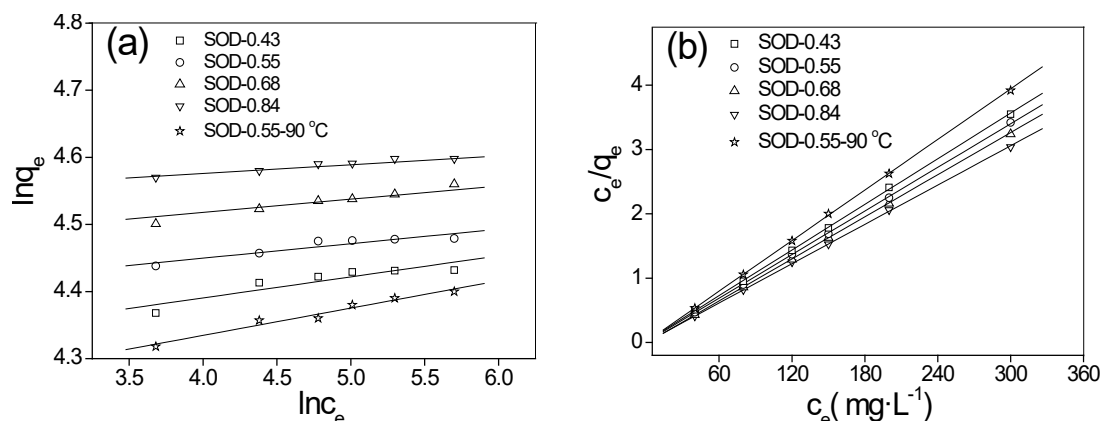


Fig. 7. Freundlich (a) and Langmuir (b) models for Cd^{2+} adsorption on the five adsorbents.

4. Conclusions

Spherical sodalite particles built of small crystallites were obtained after 10 h of room-temperature hydrothermal treatment, while with the same gel composition, the sodalite synthesized for 10 h at 90 °C was large lepispherical particles. Moreover, sodalite samples obtained at room temperature had much higher adsorption capacity, and this arose from much smaller primary particles and lower packing densities. The maximum adsorption capacities of the five sodalite crystals for Cd^{2+} decreased in the order of SOD-0.84 ($98.2 \text{ mg}\cdot\text{g}^{-1}$) > SOD-0.68 ($92.9 \text{ mg}\cdot\text{g}^{-1}$) > SOD-0.55 ($88.6 \text{ mg}\cdot\text{g}^{-1}$) > SOD-0.43 ($84.2 \text{ mg}\cdot\text{g}^{-1}$) > SOD-0.55-90 °C ($76.3 \text{ mg}\cdot\text{g}^{-1}$). The adsorption processes were best fitted to pseudo-second order kinetics, implying that Cd^{2+} adsorption occurred by chemical adsorption. The adsorption isotherms matched well with Langmuir model, suggesting that monolayer adsorption of Cd^{2+} happened on the adsorbents. In summary, sodalite samples prepared at room temperature are potential adsorbents for Cd^{2+} adsorption as low-cost materials used in water treatment in the future.

Acknowledgments

Financial Supports by the Natural Science Foundation of Henan Province, China (232300420401).

References

- [1] S. Zhang, M. Cui, J. Chen, Z. Ding, X. Wang, Y. Mu, C. Meng, *Materials Letters* 236, 233-235 (2019); <https://doi.org/10.1016/j.matlet.2018.10.100>
- [2] S. Zhang, T. Lv, Y. Mu, J. Zheng, C. Meng, *Chinese Journal of Chemical Engineering* 28 (12), 3117-3125 (2020); <https://doi.org/10.1016/j.cjche.2020.07.046>
- [3] H. Wang, Q. Chen, H. Xia, R. Liu, Y. Zhang, *Separation and Purification Technology* 328, 125074 (2024); <https://doi.org/10.1016/j.seppur.2023.125074>
- [4] S. Senniappan, S. Palanisamy, V. M. Mani, M. Umesh, C. Govindasamy, M. I. Khan, S. Shanmugam, *Environmental Research* 235, 116676 (2023); <https://doi.org/10.1016/j.envres.2023.116676>
- [5] M. E. Mahmoud, M. M. Osman, H. Abdel-Aal, G. M. Nabil, *Journal of Alloys and Compounds* 823, 153855 (2020); <https://doi.org/10.1016/j.jallcom.2020.153855>
- [6] I. V. Joseph, L. Tosheva, A. M. Doyle, *Journal of Environmental Chemical Engineering* 8 (4), 103895 (2020); <https://doi.org/10.1016/j.jece.2020.103895>

- [7] X. Cao, Z. Meng, L. Sheng, X. Hu, T. Wang, X. Sun, Y. Yu, Z. Liu, *Journal of Environmental Chemical Engineering* 11 (3), 109901 (2023); <https://doi.org/10.1016/j.jece.2023.109901>
- [8] J. Chen, R. Huang, H. Ouyang, G. Yu, Y. Liang, Q. Zheng, *Journal of Cleaner Production*, 320, 128861 (2021); <https://doi.org/10.1016/j.jclepro.2021.128861>
- [9] J. O. Dickson, J. B. Harsh, W. W. Lukens, E. M. Pierce, *Chemical Geology* 395, 138-143 (2015); <https://doi.org/10.1016/j.chemgeo.2014.12.009>
- [10] M. S. Nabavi, T. Mohammadi, M. Kazemimoghadam, *Ceramics International* 40 (4), 5889-5896 (2014); <https://doi.org/10.1016/j.ceramint.2013.11.033>
- [11] N. F. Cano, W. E. F. Ayta, S. Watanabe, *Solid State Communications* 150 (3-4), 195-197 (2010); <https://doi.org/10.1016/j.ssc.2009.10.034>
- [12] D. Zhao, A. Armutlulu, Y. Chen, Y. Wang, R. Xie, *Journal of Cleaner Production* 319, 128682 (2021); <https://doi.org/10.1016/j.jclepro.2021.128682>
- [13] C. L. Eden, M. O. Daramola, *Materialstoday: proceedings* 38 (2), 522-527 (2021); <https://doi.org/10.1016/j.matpr.2020.02.393>
- [14] M. Mahima-Kumar, H. Jena, *Microporous and Mesoporous Materials* 333, 111738 (2022); <https://doi.org/10.1016/j.micromeso.2022.111738>
- [15] O. Eterigho-Ikelegbe, S. Bada, M. O. Daramola, R. Falcon, *Materialstoday: proceedings* 38 (2), 675-681 (2021); <https://doi.org/10.1016/j.matpr.2020.03.693>
- [16] J. Zhao, L. Q. Yang, L. Yu, X. M. Zhao, Y. C. Hao, Z. J. Zhao, *Digest Journal of Nanomaterials and Biostructures* 16 (2), 527-534 (2021).
- [17] L. S. M. Nazir, Y. F. Yeong, T. L. Chew, *Colloids and Surfaces A* 600, 124803 (2020); <https://doi.org/10.1016/j.colsurfa.2020.124803>
- [18] X. Zhang, Q. Liu, S. Yang, *Digest Journal of Nanomaterials and Biostructures* 15 (3), 769-779 (2020); <https://doi.org/10.15251/DJNB.2020.153.769>
- [19] M. K. Naskar, D. Kundu, M. Chatterjee, *Materials Letters* 65 (23-24), 3408-3410 (2011); <https://doi.org/10.1016/j.matlet.2011.07.084>
- [20] J. C. Buhl, K. Schuster, L. Robben, *Microporous and Mesoporous Materials* 142 (2-3), 666-671 (2011); <https://doi.org/10.1016/j.micromeso.2011.01.020>
- [21] S. Mintova, N. H. Olson, V. Valtchev, T. Bein, *Science* 283 (5404), 958-960 (1999); <https://doi.org/10.1126/science.283.5404.958>
- [22] L. Gora, K. Strelitzky, R. W. Thompson, G. D. J. Phillis, *Zeolites* 18 (2-3), 119-131 (1997); [https://doi.org/10.1016/S0144-2449\(96\)00144-3](https://doi.org/10.1016/S0144-2449(96)00144-3)
- [23] L. Cui, R. Han, L. Yang, Y. Wu, R. Pei, F. Li, *Microporous and Mesoporous Materials* 306, 110385 (2020); <https://doi.org/10.1016/j.micromeso.2020.110385>
- [24] M. C. Manique, L. V. Lacerda, A. K. Alves, C. P. Bergmann, *Fuel* 190, 268-273 (2017); <https://doi.org/10.1016/j.fuel.2016.11.016>
- [25] Y. Lv, B. Ma, Y. Liu, C. Wang, Y. Chen, *Microporous and Mesoporous Materials* 329, 111553 (2022); <https://doi.org/10.1016/j.micromeso.2021.111553>
- [26] Z. Mo, D. Tai, H. Zhang, A. Shahab, *Chemical Engineering Journal* 443, 136320 (2022); <https://doi.org/10.1016/j.cej.2022.136320>
- [27] P. He, Y. Zhang, X. Zhang, H. Chen, *Journal of Cleaner Production* 312, 127769 (2021); <https://doi.org/10.1016/j.jclepro.2021.127769>